

Multidimensional spectroscopy with a single broadband phase-shaped laser pulse

Rachel Glenn and Shaul Mukamel

Department of Chemistry, University of California, Irvine, California 92697-2025, USA

(Dated: August 12, 2014)

Abstract

We calculate the frequency-dispersed nonlinear transmission signal of a phase-shaped visible pulse to fourth order in the field. Two phase profiles, a phase-step and phase-pulse, are considered. Two dimensional signals obtained by varying the detected frequency and phase parameters are presented for a three electronic band model system. We demonstrate how two-photon and stimulated Raman resonances can be manipulated by the phase profile and sign, and selected quantum pathways can be suppressed.

I. INTRODUCTION

Coherent control techniques, which utilize optimally shaped pulses to study the quantum interference and select quantum pathways [1–4], have been widely used to manipulate molecular structure[4–8], control chemical reactions[6, 9, 10] and to infer the electronic and vibrational motions in molecules. Pulse shaping techniques utilize the phase $\phi(\omega)$ of the field

$$\tilde{\mathcal{E}}(\omega) = \mathcal{E}(\omega)e^{i\phi(\omega)} \quad (1)$$

to control the quantum pathways in matter. Typical choices for the phase profile are an oscillating sinusoidal $\phi(\omega) = \alpha \sin(\omega - \omega_0)T$, phase-step $\phi(\omega) = \theta(\omega - \omega_0)$, or chirp $\phi(\omega) = C(\omega - \omega_0)^2$ [4, 11–14]. Another pulse shaping technique, which connects the time and frequency domain, is the use of a frequency comb[15, 16]. A frequency comb consists of a series of evenly spaced pulses in the time domain and in the frequency domain the spectrum consists of sharp lines with well defined frequencies.

Recent applications of phase control phase in one-dimensional spectroscopy have been reported. The spectral phase has been used to suppress processes such as two-photon absorption (TPA), by utilizing an asymmetric phase function[14, 17–20] with respect to the TPA transition frequency. Shaped-pulses have been employed in Raman spectroscopy[13, 18]. A phase-step, in coherent anti-Stokes Raman spectroscopy (CARS), can significantly improve the resolution and reduce the non-resonant background[18, 21–25]. By applying a non-abrupt phase-step, on the pump pulse in CARS, Raman resonances are narrower than compared to a transform limited pulse[26]. This technique[27] can be used to extract the line-width of the vibrational transitions in a molecule. Pulse-shaping utilizing a oscillating phase in CARS, allowed the Raman spectrum to be extracted with high resolution and relatively small background[28]. By applying a narrow phase-pulse, a π -gate, in single-beam CARS, the vibrational energy levels were mapped in a single measurement[29]. Note that Ref. [29] used an abrupt phase-pulse, where here we study a non-abrupt phase-pulse.

Coherent control is carried out using an adaptive (closed loop) pulse shaping scheme that employs genetic algorithm to optimize many control parameters[30–35] of the laser pulses[36]. Here we use a few control paramters.

In this paper, we extend these applications to two-dimensional spectroscopy by plotting the transmission spectrum of a broadband pulse as a function of the dispersed frequency and the position of a phase-step or a phase-pulse. A phase-step and phase-pulse have been widely used in

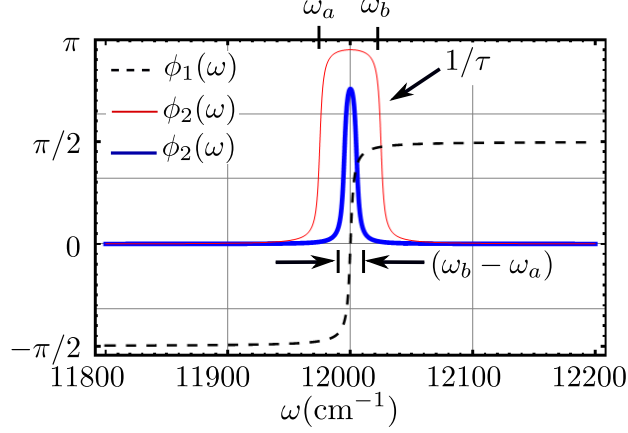


FIG. 1: (Color online) The spectral phase $\phi(\omega)$ that we consider, (dashed-black) is a phase step, Eq. (15) with transition width $1/\tau_a = 2\text{cm}^{-1}$; (thick-blue) a narrow phase-pulse, Eq. (18), with $\omega_a = 11995\text{cm}^{-1}$, $\omega_b = 12005\text{cm}^{-1}$, $\tau = 0.5\text{cm}$; (thin-red) a wide phase-pulse, Eq. (18), $\omega_a = 11975\text{cm}^{-1}$, $\omega_b = 12025\text{cm}^{-1}$, $\tau = 0.5\text{cm}$.

one-dimensional spectroscopy[18, 21–28, 31, 37]. We investigate the control of the quantum pathways in the transmission of a single broadband pulse using the phase-pulse and phase-step shown in Fig. 1. The two-dimensional transmission signal for the phase-pulse and step show diagonal peaks corresponding to two-photon absorption, Stokes processes, and Rayleigh processes. The two-photon absorption and Stokes peaks are sensitive to the the sign of the phase.

II. THE QUARTIC TRANSMISSION SPECTRUM OF A THREE-BAND MODEL

We consider a three band system (Fig. 2) with electronic states $|g\rangle$, $|e\rangle$, $|f\rangle$ coupled to the radiation field and described by the Hamiltonian

$$\hat{H} = \hat{H}_e + \hat{H}_{int}, \quad (2)$$

where

$$\hat{H}_e = \sum_{\nu=g_i, e_i, f_i} \hbar\epsilon_\nu |\nu\rangle\langle\nu|, \quad (3)$$

represents the system and $\hbar\epsilon_\nu$ is the energy of the state ν . The level scheme was chosen to highlight the resonances affected by the phase. \hat{H}_{int} is the field-matter dipole interaction, with the dipole operator $\hat{\mu} = \hat{V}^\dagger + \hat{V}$, where V^\dagger (V) is the matter raising and (lowering) operator, so that $V(t) = \sum_e V_{ge}(t)|g\rangle\langle e| + \sum_f V_{ef}(t)|e\rangle\langle f|$ and $V_{ij}(t)$ is the dipole matrix element in the interaction picture.

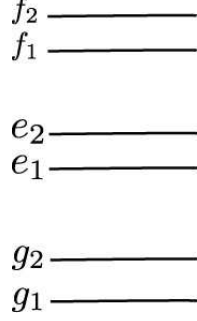


FIG. 2: (Color online) The model level scheme, the corresponding energy levels are $g_1 = 0\text{cm}^{-1}$, $g_2 = 75\text{cm}^{-1}$, $e_1 = 12025\text{cm}^{-1}$, $e_2 = 12050\text{cm}^{-1}$, $f_1 = 24125\text{cm}^{-1}$, $f_2 = 24150\text{cm}^{-1}$. The dephasing rates were all chosen to be the same, $\gamma = 10\text{cm}^{-1}$.

The classical electric field is $E(t) = \tilde{\mathcal{E}}(t) + \tilde{\mathcal{E}}^\dagger(t)$. In the rotating wave approximation we have

$$\hat{H}_{int} = -(\tilde{\mathcal{E}}^\dagger(t)V(t) + \tilde{\mathcal{E}}(t)V^\dagger(t)). \quad (4)$$

We shall calculate the frequency dispersed transmitted signal[38]

$$S(\omega) = -\frac{2}{\hbar}\mathcal{I}\left[\tilde{\mathcal{E}}^\dagger(\omega)\int_{-\infty}^{\infty}dt\langle V_L(t)e^{-\frac{i}{\hbar}\int_{-\infty}^{\infty}H_{int-}(T)dT}\rangle e^{i\omega t}\right], \quad (5)$$

where $\mathcal{I}A(\omega)$ denotes the imaginary part of $A(\omega)$ and $\tilde{\mathcal{E}}^\dagger(\omega)$ is the Fourier transform: $\tilde{\mathcal{E}}^\dagger(\omega) = \int_{-\infty}^{\infty}dt\mathcal{E}^\dagger(t)e^{i\omega t}$. We use the superoperator formalism [39]. The superoperator H_{int-} is defined as $H_{int-} = H_{intL} - H_{intR}$. The two superoperators H_{intL} and H_{intR} are defined by their actions $H_{intL}X = H_{int}X$ and $H_{intR}X = XH_{int}$ [39]. The field is represented by its amplitude $\mathcal{E}(\omega)$ and phase $\phi(\omega)$, Eq. (1).

The linear absorption spectrum is obtained by expanding Eq. (5) to first-order in H_{int-}

$$S(\omega) = -|\tilde{\mathcal{E}}(\omega)|^2\mathcal{I}\chi^{(1)}(\omega), \quad (6)$$

where the linear susceptibility is

$$\chi^{(1)}(\omega) = \sum_{e_1} -\frac{1}{\hbar}|\mu_{e_1g_1}|^2 G_{e_1g_1}(\omega), \quad (7)$$

the Green's function is $G_{e_1g_1}(\omega) = (\omega - \omega_{e_1g_1} + i\gamma)^{-1}$ and γ is the dephasing rate. We use a Gaussian electric field

$$\mathcal{E}(\omega; \Omega_1, \sigma_1) = e^{-(\omega - \Omega_1)^2 / (2\sigma_1^2)}, \quad (8)$$

with center frequency Ω_1 and standard deviation σ_1 . The pulse power spectrum, $|\tilde{\mathcal{E}}(\omega)|^2$, Eq. (1) with a Gaussian pulse, Eq. (8), is shown in Fig. 3(c). Equation (6) is plotted in Fig. 3(a), with the dipole moments and \hbar are set to one. The two peaks in Fig. 3(a) correspond to the transition frequencies $\omega_{e_1g_1}$ and $\omega_{e_2g_1}$.

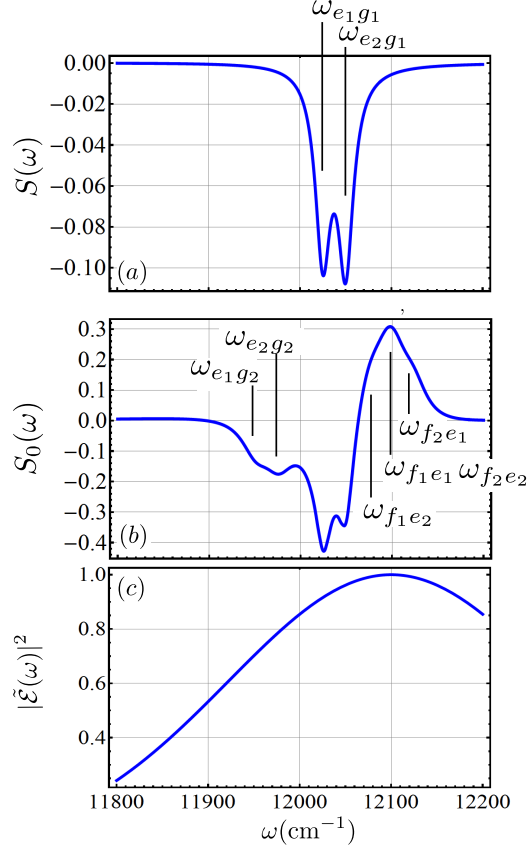


FIG. 3: (Color online) (a) The linear absorption Eq. (6) of the model system of Fig. 2. (b) The frequency dispersed transmission signal $S_0(\omega)$, Eq. (14). (c) The pulse power spectrum, $|\tilde{\mathcal{E}}(\omega)|^2$, from Eq. (1). We used a Gaussian pulse Eq. (8) with $\phi = 0$ for the field, Eq. (1), $\sigma = 252\text{cm}^{-1}$ and $\Omega_1 = 12100\text{cm}^{-1}$.

The ladder diagram expansion of Eq. (5) to third-order in H_{int} is shown in Fig. 4. The transmission signal[38] is given as

$$S(\omega) = \frac{2}{\hbar} \mathcal{I} \int_{-\infty}^{\infty} \int_{-\infty}^{\infty} d\omega_1 d\omega_2 \tilde{\mathcal{E}}^*(\omega) \tilde{\mathcal{E}}(\omega_1) \tilde{\mathcal{E}}^*(\omega_2) \tilde{\mathcal{E}}(\omega - \omega_1 + \omega_2) 2\pi \chi^{(3)}(-\omega; -\omega_2, \omega_1, \omega - \omega_1 + \omega_2). \quad (9)$$

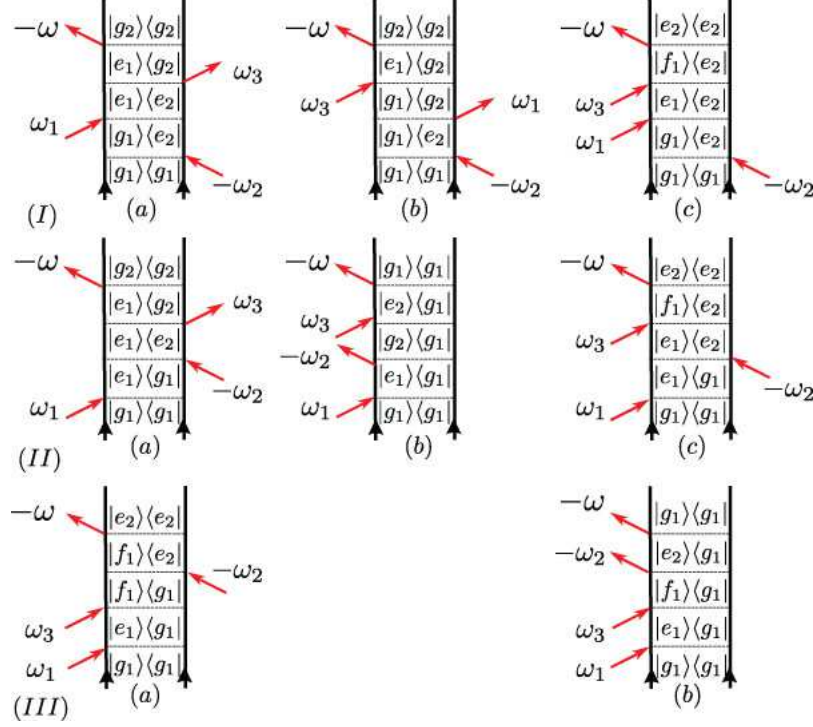


FIG. 4: (Color online) Ladder diagrams for the frequency dispersed transmitted signal Eq. (5) expanded to third-order in H_{int} from a single pulse. The frequencies ω_1 and ω_2 correspond the variables ω_1, ω_2 in the susceptibility, Eq. (10).

The third-order susceptibility is

$$\begin{aligned} \chi^{(3)}(-\omega; -\omega_2, \omega_1, \omega - \omega_1 + \omega_2) &= \chi_I^{(3)}(-\omega; -\omega_2, \omega_1, \omega - \omega_1 + \omega_2) \\ &+ \chi_{II}^{(3)}(-\omega; -\omega_2, \omega_1, \omega - \omega_1 + \omega_2) + \chi_{III}^{(3)}(-\omega; -\omega_2, \omega_1, \omega - \omega_1 + \omega_2), \end{aligned} \quad (10)$$

where the three terms correspond to diagrams (I), (II), (III) in Fig. 4.

$$\begin{aligned} \chi_I^{(3)}(-\omega; -\omega_2, \omega_1, \omega - \omega_1 + \omega_2) &= \left(\frac{-1}{2\pi\hbar}\right)^3 \sum_{e_1, e_2, g_2, f_1} V_{g_1 e_2} V_{g_1 e_1}^* V_{e_2 g_2}^* V_{e_1 g_2} G_{e_2 g_1}(\omega_2) G_{e_1 e_2}(\omega_1 - \omega_2) G_{e_1 g_2}(\omega) \\ &+ V_{g_1 e_2} V_{e_2 g_2}^* V_{g_1 e_1}^* V_{e_1 g_2} G_{e_2 g_1}(\omega_2) G_{g_1 g_2}(\omega_1 - \omega_2) G_{e_1 g_2}(\omega) \\ &- V_{g_1 e_2} V_{g_1 e_1}^* V_{e_1 f_1}^* V_{f_1 e_2} G_{e_2 g_1}(\omega_2) G_{e_1 e_2}(\omega_1 - \omega_2) G_{f_1 e_2}(\omega), \end{aligned} \quad (11)$$

$$\begin{aligned} \chi_{II}^{(3)}(-\omega; \omega_1, -\omega_2, \omega - \omega_1 + \omega_2) &= \left(\frac{-1}{2\pi\hbar}\right)^3 \sum_{e_1, e_2, g_2, f_1} V_{g_1 e_1}^* V_{g_1 e_2} V_{e_2 g_2}^* V_{e_1 g_2} G_{e_1 g_1}(\omega_1) G_{e_1 e_2}(\omega_1 - \omega_2) G_{e_1 g_2}(\omega) \\ &+ V_{g_1 e_1}^* V_{e_1 g_2} V_{g_1 e_2}^* V_{e_2 g_1} G_{e_1 g_1}(\omega_1) G_{g_1 g_2}(\omega_1 - \omega_2) G_{e_2 g_1}(\omega) \\ &- V_{g_1 e_1}^* V_{g_1 e_2} V_{e_1 f_1}^* V_{f_1 e_2} G_{e_1 g_1}(\omega_1) G_{e_1 e_2}(\omega_1 - \omega_2) G_{f_1 e_2}(\omega), \end{aligned} \quad (12)$$

$$\begin{aligned} \chi_{III}^{(3)}(-\omega; \omega_1, \omega - \omega_1 + \omega_2, -\omega_2) = & \left(\frac{-1}{2\pi\hbar} \right)^3 \sum_{e_1, e_2, g_2, f_1} V_{g_1 e_1}^* V_{e_1 f_1}^* V_{f_1 e_2} V_{e_2 g_1} G_{e_1 g_1}(\omega_1) G_{f_1 g_1}(\omega + \omega_2) G_{e_2 g_1}(\omega) \\ & - V_{g_1 e_1}^* V_{e_1 f_1}^* V_{g_1 e_2} V_{f_1 e_2} G_{e_1 g_1}(\omega_1) G_{f_1 g_1}(\omega + \omega_2) G_{f_1 e_2}(\omega). \end{aligned} \quad (13)$$

An alternative form for the susceptibility derived using the loop diagrams is given in Appendix A. They represent the wavefunction in Hilbert-space, instead of the density matrix, so that γ in Hilbert space represents the inverse lifetime. Equations (A2)-(A5), contain fewer terms to integrate compared to the Liouville-space. However, it is easier to perform the numerical integration in Eq. (9), using Mathematica in Liouville-space than in Hilbert-space. For this reason, we use the Liouville-space representation.

The total transmission spectrum of an unshaped transform limited pulse with $\phi = 0$,

$$S_0(\omega) = S(\omega, \phi(\omega) = 0), \quad (14)$$

is shown in Fig. 3(b). The transition frequencies are marked, based on the energy level diagram Fig. 2. The two absorption peaks at $\omega = \omega_{e_1 g_1}, \omega_{e_2 g_1}$ in Figs. 3(b), correspond to the Rayleigh process, where as, $\omega_{e_1 g_2}, \omega_{e_2 g_2}$ represent the Stokes process. $\omega_{e_1 g_1}, \omega_{e_2 g_1}$ are the most pronounced; they are also seen in the linear signal in Fig. 3(a). The four emission peaks at $\omega = \omega_{f_1 e_1}, \omega_{f_2 e_1}, \omega_{f_1 e_2}$ and $\omega_{f_2 e_2}$ in Figs. 3(b) correspond to two-photon absorption. The $\omega_{f_1 e_2}$ peak is difficult to distinguish due to the transition from an absorption to an emission near that wavelength. In Appendix B, we separate $S_0(\omega)$ into three components $S_0^I(\omega), S_0^{II}(\omega), S_0^{III}(\omega)$, corresponding to $\chi_I^{(3)}, \chi_{II}^{(3)}, \chi_{III}^{(3)}$. These are plotted in Fig. 13.

III. TWO DIMENSIONAL NONLINEAR TRANSMISSION SIGNAL WITH A PHASE-STEP

We first consider a π -phase-step phase

$$\phi_1(\omega) = \arctan[\tau_a(\omega - \omega_a)], \quad (15)$$

which has finite transition τ_a , and position ω_a , as marked in Fig. 1. The phase-step in Fig. 1 has transition width $1/\tau_a = 2\text{cm}^{-1}$.

The integrals in Eq. (9) were calculated numerically, with Gaussian pulses, Eq. (8), $\sigma_1 = 252\text{cm}^{-1}$, $\Omega_1 = 12100\text{cm}^{-1}$ and the dipole moments set to one.

The two-dimensional frequency dispersed transmission signal

$$\Delta S_{\text{step}}(\omega; \omega_a) = S(\omega; \phi_1(\omega, \omega_a, \tau_a)) - S_0(\omega), \quad (16)$$

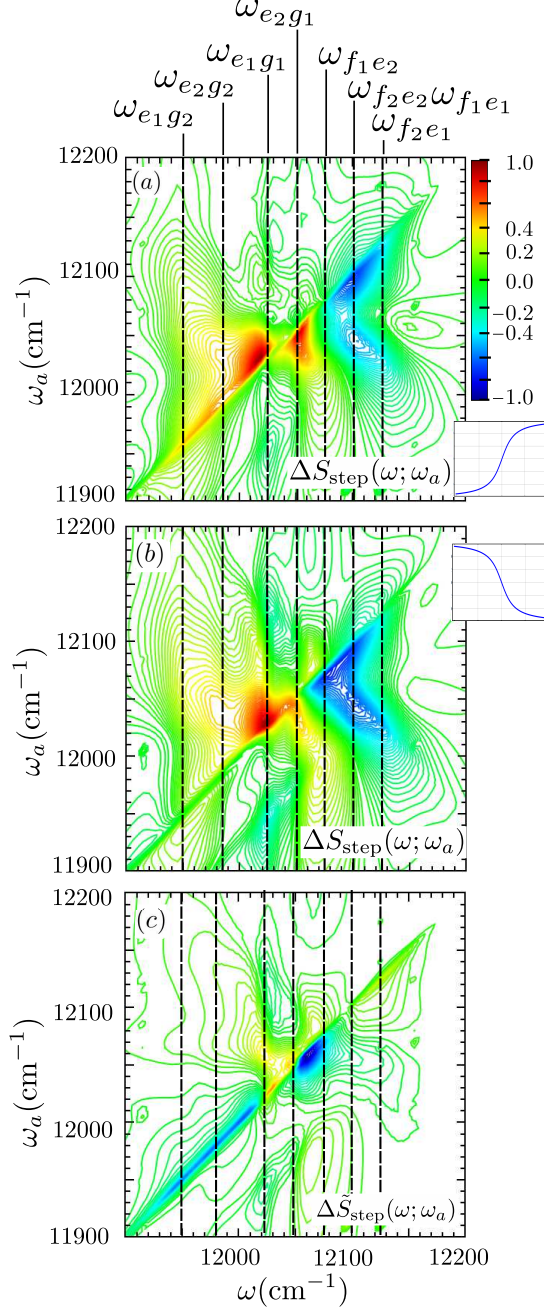


FIG. 5: (Color online) The two-dimensional frequency dispersed transmission signal $\Delta S_{\text{step}}(\omega, \omega_a)$, Eq. (16), with phase $\phi_1(\omega, \omega_a)$ is plotted; (a) $\tau_a = 0.5\text{cm}$; (b) $\tau_a = -0.5\text{cm}$. (c) The difference between (a) and (b), $\Delta \tilde{S}_{\text{step}}(\omega, \omega_a)$, Eq. (17). The vertical dashed-black lines mark the transition frequencies. The insets show the shape of the phase-step.

is plotted in Fig. 5(a) for a positive phase-step $\tau_a = 0.5\text{cm}$. The vertical black-dashed lines mark the positions of the transition peaks. The spectra contains diagonal peaks that extend above and below the diagonal line at $\omega = \omega_a$. The main diagonal peaks are at $\omega = \omega_{e1g1}, \omega_{e2g1}, \omega_{f1e1}$ and

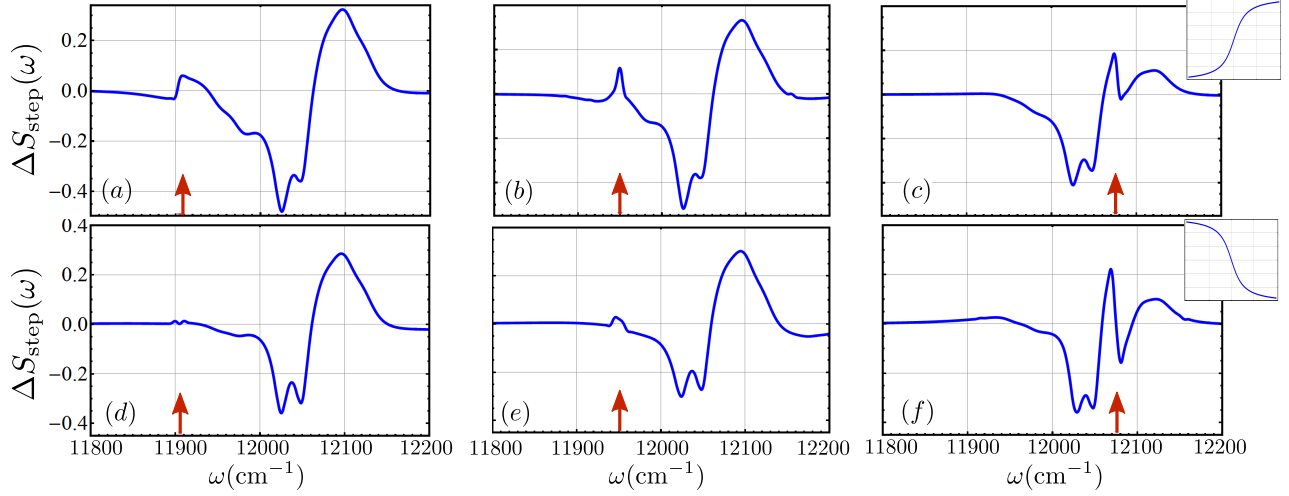


FIG. 6: (Color online) The transmission signal, Eq. (9), using a phase-step, $\phi_1(\omega, \omega_a)$. Top-row: positive-step, $\tau_a = 0.5\text{cm}$, (a) $\omega_a = 11905\text{cm}^{-1}$, (b) $\omega_a = \omega_{e_2g_2}$, (c) $\omega_a = \omega_{f_1e_1}$. Bottom-row: negative phase-step, $\tau_a = -0.5\text{cm}$, (d) $\omega_a = 11905\text{cm}^{-1}$, (e) $\omega_a = \omega_{e_2g_2}$, (f) $\omega_a = \omega_{f_1e_1}$. The red arrows marks the position of the phase-step. The insets show the shape of the phase-step.

$\omega_{e_1g_2} < \omega < \omega_{e_2g_2}$. These peaks correspond to the peaks in Fig. 3(b). The phase-step changes the Rayleigh and Stokes peaks from absorption to emission, and the TPA peaks change from emission to absorption. As seen in Fig. 3(b), the Stokes peaks appear weaker than the other transition peaks in the spectra. These peaks appear above the diagonal line. They originate from the ladder diagrams (I)(a)(b) and (II)(a) in Fig. 4. Diagrams (I)(b) and (II)(a) have the time sequence of arrows which alternate in directions and diagram (I)(a) has the time sequence of two successive arrows with the same direction. The $\omega = \omega_{e_1g_1}$ peak extends above the diagonal line, while the $\omega = \omega_{e_2g_1}$ extends below the diagonal line. The main contribution for the $\omega = \omega_{e_1g_1}$ peak comes from ladder diagrams Fig. 4(I)(a) (b), (II)(a)(b). The dominant contribution is from diagrams (II)(a),(b) which have alternating time-ordering of the arrows direction. The main contribution to $\omega = \omega_{e_2g_1}$ peak is from the diagram (III)(b), which has two successive arrows in the same direction. The $\omega = \omega_{f_2e_1}, \omega_{f_1e_2}, \omega_{f_1e_1}$ peaks appear below the diagonal line. These peaks can be traced back to diagrams (I)(c), (II)(c), (III)(a) in Fig. 4, all of which have a time sequence of two successive arrows in the same direction. Overall, the peaks that extend below the diagonal line, have a dominate contribution from the diagrams which contain time ordering of two successive arrows with the same direction and peaks that extend above the diagonal line have a dominate contribution from the time sequence of arrows which alternate in direction.

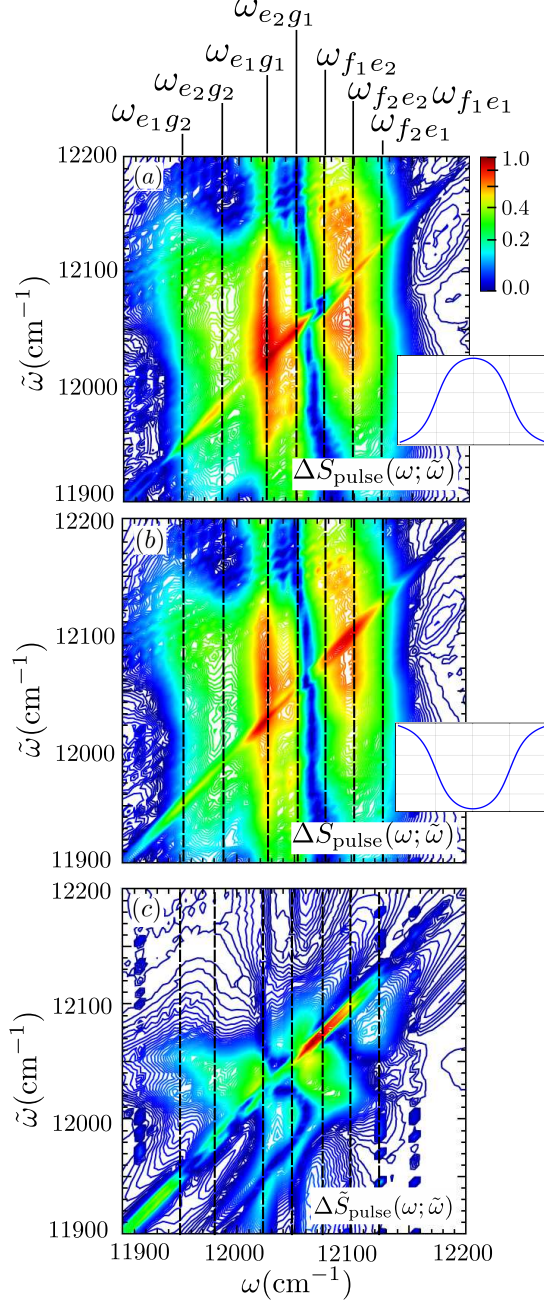


FIG. 7: (Color online) The two-dimensional frequency dispersed transmission signal Eq. (19) is plotted with a narrow phase-pulse, $\phi_2(\omega, \tilde{\omega})$ width $\Delta\omega = 10\text{cm}^{-1}$; (a) $\tau_a = 0.5\text{cm}$, (b) $\tau_a = -0.5\text{cm}$. (c) The difference between between (a), (b), Eq. (20). The insets show the shape of the phase-pulse.

In Fig. 14 of Appendix B, we separate the transmission signal Fig. 5 into the components $S_I(\omega, \omega_a)$, $S_{II}(\omega, \omega_a)$ and $S_{III}(\omega, \omega_a)$, corresponding to $\chi_I^{(3)}$, $\chi_{II}^{(3)}$, $\chi_{III}^{(3)}$ in Eq. (10). The signal components, show off-diagonal peaks, which appear when ω_a coincides with the transition fre-

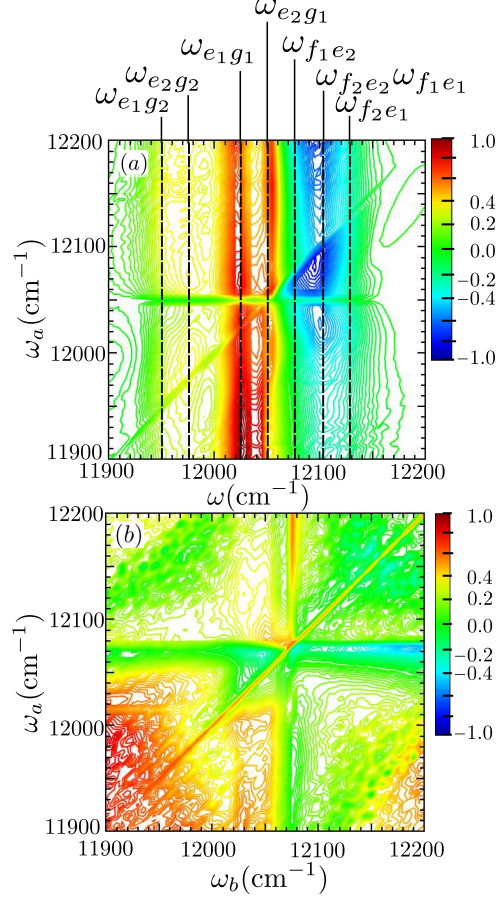


FIG. 8: (Color online) (a) The two-dimensional transmission signal, Eq. (21), is plotted for $\phi_2(\omega, \omega_a, \omega_{e2g1})$ with $\tau = -0.5\text{cm}$. (b) The 2D transmission spectrum with phase $\phi_2(\omega, \omega_a, \omega_b)$, Eq. (9), vs phase-step positions ω_a and ω_b , is plotted for $\tau = -0.5\text{cm}$ and $\omega = \omega_{f2e1}$

quencies. These peaks are small compared to the diagonal peaks. From Fig. 14, it can be seen that the transmission signal with a phase-step is mostly composed of the $S_{II}(\omega, \omega_a)$ and $S_{III}(\omega, \omega_a)$ components.

The transmission signal with a negative phase-step $\tau_a = -0.5\text{cm}$, Eq. (16), is shown in Fig. 5(b). The diagonal $\omega = \omega_{e1g2}, \omega_{e2g2}$ peaks are much weaker, compared to the positive phase-step. However, the diagonal $\omega = \omega_{f1e1}, \omega_{f1e2}, \omega_{f2e1}$ peaks appear stronger, than with the positive phase-step. These peaks originate from diagrams in Fig. 4(I)(c), (II)(c), (III)(a). This shows that the negative going phase-step enhances the TPA diagonal peaks stronger, whereas, a positive going phase-step enhances the $\omega = \omega_{e1g2}, \omega_{e2g2}$ peaks better.

The difference of the transmission signal with a negative and positive phase-step

$$\Delta\tilde{S}_{\text{step}}(\omega; \omega_a) = S(\omega; \phi_1(\omega, \omega_a, -\tau_a)) - S(\omega; \phi_1(\omega, \omega_a, \tau_a)) \quad (17)$$

is plotted in Fig. 5(c). It shows peaks along the diagonal line. The spectral phase function can be written as the sum of an even and odd function, $\exp(i \arctan(\pm x)) = (1 \pm x)/\sqrt{1+x^2}$. The difference in the transmission signal with a positive and negative phase-step gives the amplification by the odd part of the spectral phase function $-2x/\sqrt{1+x^2}$. Figure 5(c) confirms that the positive going phase-step enhances the $\omega = \omega_{e_1g_2}, \omega_{e_2g_2}$ peaks better than the negative going, while the negative going phase-step enhances the $\omega = \omega_{f_1e_1}, \omega_{f_1e_2}, \omega_{f_2e_1}$ peaks better than the positive. This effect is more clearly seen in the one-dimensional transmission spectra $S(\omega; \phi_1(\omega, \omega_a))$, Eq. (9), in Fig. 6. Positive step spectra are shown in the top row of Fig. 6 for three phase-step positions. The off-resonant phase-step position $\omega_a = 11905\text{cm}^{-1}$ in (a) shows that the background is amplified. When the phase-step coincides with a transition frequency $\omega_a = \omega_{e_1g_2}$ in (b) the peak becomes amplified and the resolution is increased. This is because the Greens functions, $G_\beta(\omega) = (\omega - \omega_\beta + i\gamma)^{-1}$ in Eq. (11)-(13) inverts the phase over a width γ about the resonance frequency $\omega = \omega_\beta$. The application of the phase-step at $\omega_a = \omega_\beta$ inverts the phase again over a width $1/\tau_a$, enhancing the peak. This was demonstrated by Oron et al.[26] in a CARS experiment. Fig. 6(c) shows the enhancement of the TPA at $\omega_{f_1e_2}$. The negative phase-step is plotted in the bottom row of Fig. 6 for three values of the phase-step position. For the phase-step off resonant, $\omega_a = 11905\text{cm}^{-1}$, (d) there is little amplification of the background. When $\omega_a = \omega_{e_1g_2}$ in (e), the enhancement becomes clear. The negative step enhances the TPA $\omega_{f_1e_2}$, in (f), better than the Stokes peak. Fig. 6(b) shows that the positive step narrows and amplifies the Stokes peak at $\omega_a = \omega_{e_1g_2}$ better than the negative (e). However, the negative step in (f) enhances the TPA at $\omega_a = \omega_{f_1e_2}$ better than the positive and that this peak is enhanced down-ward where as the $\omega_s = \omega_{e_1g_2}$ peak is enhanced up-ward.

In this study, we only considered homogeneous broadening. Inhomogeneous broadening changes the line-shapes of the peaks from diagrams (I) in Fig. 4 from symmetric to asymmetric[38]. The line-shapes from diagrams (II) and (III) in Fig. 4 remain symmetric with inhomogeneous broadening[38]. The transmission signal with the phase-step is dominated by the transition peaks from diagrams (II) and (III) in Fig. 4, so we expect inhomogeneous broadening to have little effect on the phase-step.

IV. TWO DIMENSIONAL TRANSMISSION SIGNAL WITH A PHASE-PULSE

We next present simulations which use a π -phase-pulse spectral phase

$$\phi_2(\omega, \omega_a, \omega_b) = \arctan[\tau(\omega - \omega_a)] - \arctan[\tau(\omega - \omega_b)]. \quad (18)$$

The pulse lies between ω_a and ω_b , with transition steepness τ . We first consider a narrow phase-pulse, with width close to the transition width of the step, see Fig. 1. does not give a full π -inversion. A full π -inversion is achieved with a wider phase-pulse, $\omega_a - \omega_b = 50\text{cm}^{-1}$ thin-red line in Fig. 1.

The transmission spectrum for a narrow phase-pulse

$$\Delta S_{\text{pulse}}(\omega; \tilde{\omega}) = S(\omega; \phi_2(\omega, \tilde{\omega} + \frac{\Delta\omega}{2}, \tilde{\omega} - \frac{\Delta\omega}{2}, \tau)) - S_0(\omega), \quad (19)$$

with width $\Delta\omega = 10\text{cm}^{-1}$ and position $\tilde{\omega}$ is displayed in Fig. 7(a) for a positive going pulse, $\tau = 0.5\text{cm}$. The vertical dashed-black lines mark the position of the transition peaks. The positive going pulse in Fig. 7(a) has three vertically spread peaks at $\omega = \omega_{e_1g_2}, \omega_{e_1g_1}, \omega_{f_1e_2}$, corresponding to the three well pronounced peaks in Fig. 3(b). The effect of the phase-step changed the absorption peaks in Fig. 3(b) to emission peaks and vice versa. The effect of the phase-pulse gives the same affect. The data in Fig. 7 is plotted on a scale, which gives the best visibility for peaks in the transmission spectrum. The main contribution to the transmission signal can be traced back to the diagrams (I) in Fig. 4. See Fig. 15 in the Appendix B for the individual $\Delta S_{\text{pulse}}^I(\omega)$, $\Delta S_{\text{pulse}}^{II}(\omega)$ and $\Delta S_{\text{pulse}}^{III}(\omega)$ components. Signal component $\Delta S_{\text{pulse}}^{II}(\omega, \omega_a)$ in Fig. 15 contributes two diagonal peaks near $\omega = \omega_{e_2g_1}, \omega_{f_1e_1}$ and $\Delta S_{\text{pulse}}^{III}(\omega, \omega_a)$ contribution is not noticeable.

The negative going phase-pulse $\tau = -0.5\text{cm}$, Eq. (19), is shown in Fig. 7(b). The spectra are dominated by the contributions from diagrams (I) in Fig. 4. The signal $\Delta S_{\text{pulse}}^{II}(\omega, \omega_a)$ contributes two diagonal peaks at $\omega = \omega_{e_1g_1}, \omega_{f_1e_1}$ and $\Delta S_{\text{pulse}}^{III}(\omega, \omega_a)$ contribution is not noticeable. This shows that the positive or negative narrow phase-pulse can be used to suppress the contributions from diagrams (II) and (III) in the transmission spectra. Note that with inhomogeneous broadening included the signal with a phase-pulse should be significantly affected, since it is dominated by the diagrams (I). The negative pulse enhances the diagonal peak near $\omega = \omega_{f_1e_1}$ better than the positive pulse. It appears that the positive pulse enhances the $\omega = \omega_{e_1g_2}, \omega_{e_2g_2}$ better than the negative.

The difference in the transmission signal for a negative and positive pulse

$$\Delta \tilde{S}_{\text{pulse}}(\omega; \tilde{\omega}) = S(\omega; \phi_2(\omega, \tilde{\omega} + \frac{\Delta\omega}{2}, \tilde{\omega} - \frac{\Delta\omega}{2}, -\tau)) - S(\omega; \phi_2(\omega, \tilde{\omega} + \frac{\Delta\omega}{2}, \tilde{\omega} - \frac{\Delta\omega}{2}, \tau)) \quad (20)$$

is plotted in Fig. 7(c). The spectra is composed a diagonal peak near $\omega = \omega_{f_1 e_1}$ and two small diagonal peaks at $\omega = \omega_{e_2 g_2}, \omega_{e_1 g_2}$. The two-dimensional spectra most resembles the Fig. 15(f) from diagrams (II).

We have explored if a variable pulse width $\phi_2(\omega, \omega_a, \omega_b)$ with a negative-step located at $\omega_b = \omega_{e_2 g_1}$ could better enhance the peaks. The $\omega = \omega_{e_2 g_1}$ peak appeared strong for a positive/negative narrow-phase-pulse or step and always remained above the diagonal line. It is interesting to see if there is any sensitivity to the phase-step position. The transmission spectrum

$$\Delta S_{\text{pulse}}(\omega; \omega_a) = S(\omega; \phi_2(\omega, \omega_a, \omega_b, \tau)) - S_0(\omega). \quad (21)$$

with a variable pulse width is shown in Fig. 8(a). This creates a negative-going pulse for $\omega_a < \omega_{e_2 g_1}$ and positive-going pulse for $\omega_a > \omega_{e_2 g_1}$. The horizontal line at $\omega_a = \omega_b$ is where both phase-steps coincide and their effect vanishes. The $\omega = \omega_{e_2 g_1}$ peak is well pronounced away from the diagonal line, for any value of the pulse width. Notice that the $\omega = \omega_{f_1 e_2}, \omega_{f_2 e_2}$ peaks become strongly enhanced when the pulse changes from a negative to a positive going pulse. Compare to the narrow-pulse Fig 7, the variable width enhances the $\omega = \omega_{f_1 e_2}, \omega_{f_2 e_2}$ diagonal peaks stronger. This is because the pulse is composed of a negative step located at ω_a .

The phase-pulse has been used to enhance the TPA peaks $\omega_{f_i e_j}$ in the spectrum, involving an intermediate resonant state[40]. Two opposite phase-steps located at the two transition frequencies, $\omega_{e_j g_1}$ and $\omega_{f_i e_j}$ involved in the TPA transition $\omega_{f_i g_1}$ where used. If the intermediate state is located at $\omega_{f_i g_1}/2$, the phase-pulse would have zero width. When the intermediate resonant state is de-tuned from $\omega_{f_i g_1}/2$ the phase-pulse has finite width and can be employed to enhance the TPA peak. We searched for a particular width that would selectively enhance the TPA peak $\omega_{f_1 e_1}$ in the transmission spectrum. The two-dimensional spectra, Eq. (9), with phase $\phi_2(\omega, \omega_a, \omega_b)$, are plotted in Fig. 8(b) as a function of ω_a and ω_b , for $\omega = \omega_{f_1 e_2}$. The diagonal line at $\omega_a = \omega_b$ is where width of the phase-pulse is zero. The phase-pulse is positive going for $\omega_b > \omega_a$ and negative going for $\omega_a > \omega_b$. The diagonal peak at $\omega_a = \omega_b = \omega_{f_1 e_2}$ shows that $\omega = \omega_{f_1 e_2}$ is optimized by employing a narrow negative pulse. There is one horizontal line for $\omega_b > \omega_a$ and $\omega_a = \omega_{f_1 e_2}$. This is a wide pulse with the negative going step at $\omega_a = \omega_{f_1 e_2}$. There is a vertical line for $\omega_a > \omega_b$ and $\omega_b = \omega_{f_1 e_2}$, which is again a wide pulse with a negative step located at $\omega_b = \omega_{f_1 e_2}$. Recall that in Fig. 5(b) the transition peak $\omega_{f_1 e_2}$ was well enhanced using a negative step rather than a positive. There are several regions where the background becomes pronounced: the bottom right and left corners. For $\omega > \omega_{f_1 e_2}$, the background is minimal. Overall, the spectra does not show

any favorable width for a wide pulse.

We next chose, the width of the phase-pulse to coincide with the transition frequencies involved in the TPA transition $\omega_{f_1g_1}$, with a phase-pulse centered at $\omega_{f_1g_1}/2$. See the inset of Fig. 9. The transmission signal $S_{\text{pulse}}(\omega)$, Eq. (9), is plotted with a positive phase-pulse (blue-thick) and a negative phase-pulse (thin-red). Overall, the positive phase-pulse amplifies the TPA better than the negative phase-pulse. This is because the positive phase-pulse is composed of a negative step at $\omega_b = \omega_{f_1e_2}$, while the negative phase-pulse is composed of a positive step at $\omega_b = \omega_{f_1e_2}$.

In Fig. 10, we compare all three profiles for selectively enhancing the peak $\omega_{f_1e_2}$. The thick-blue line in Fig. 10 is the transmission signal, Eq. (9) with negative phase-step, $\phi_1(\omega, \omega_{f_1e_2})$. The thin-red line corresponds to the transmission signal, Eq. (9) with a negative narrow-phase-pulse $\phi_2(\omega, \omega_{f_1e_2} + \frac{1}{2}\Delta\omega, \omega_{f_1e_2} - \frac{1}{2}\Delta\omega)$, with width $\Delta\omega = 10\text{cm}^{-1}$. The dashed-black line in the transmission signal is a positive wide-phase pulse $\phi_2(\omega, \omega_{e_1g_1}, \omega_{f_1e_2})$, shown in the inset of Fig. 9. Figure 10 shows that the phase-step gives the best enhancement. The phase-step centered at the resonant frequency inverts the phase to compensate for the phase inversion of the Green's function and enhances the peak [26]. The wide and narrow phase-pulses provide comparable enhancement.

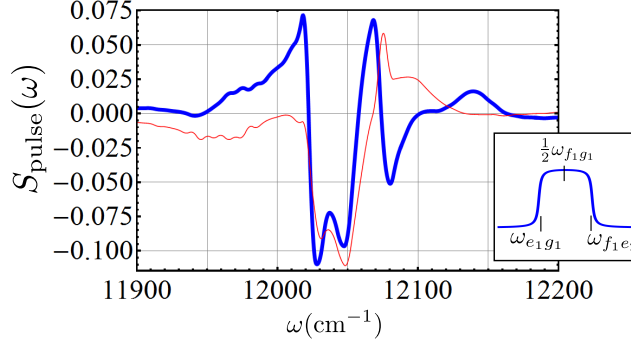


FIG. 9: (Color online) The transmission signal Eq. (9) $\phi_2(\omega, \omega_{e_1g_1}, \omega_{f_1e_2})$ is plotted for a (thick-blue) positive phase-pulse, $\tau = 0.5\text{cm}$ and a (thin-red) negative phase-pulse $\tau = -0.5\text{cm}$.

The width and position of the pulse used are shown in the inset.

V. OFF-RESONANT STIMULATED RAMAN SIGNALS

We now set the carrier frequency of the pulse to be off-resonant at $\Omega_1 = 8000\text{cm}^{-1}$. The transmission signal, Eq. (9), with a positive phase-step is shown in Fig. 11(a) for three values of

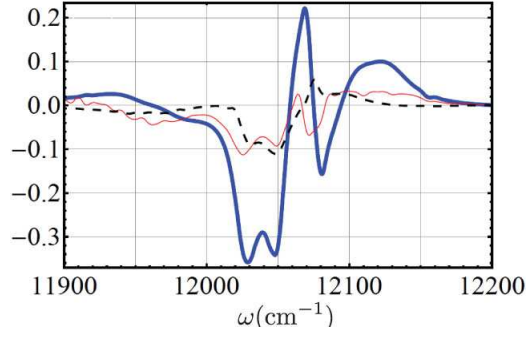


FIG. 10: (Color online) Three profiles for amplifying the peak $\omega_{f_1 e_2}$ in the transmission spectrum

Eq. (9) are compared; (thick-blue) phase-step, $\phi_1(\omega, \omega_{f_1 e_2})$; (thin-red) narrow-phase-step $\phi_2(\omega, \omega_{f_1 e_2} + \frac{1}{2}\Delta\omega, \omega_{f_1 e_2} - \frac{1}{2}\Delta\omega)$, with width $\Delta\omega = 10\text{cm}^{-1}$; (dashed-black) wide-phase-pulse $\phi_2(\omega, \omega_{e_1 g_1}, \omega_{f_1 e_2})$.

ω_a . The black dashed line is the transmission signal, Eq. (14) without pulse shaping, $\phi = 0$. With the phase-step, the transmission spectra shows a peak at $\omega = \omega_a$ with a width close to $\omega_{g_2 g_1}$.

The transmission signal with a negative phase-step, Eq. (9), with $\tau_a = -0.5$, is shown in Fig. 11(b) for three values of ω_a . The spectra show a peak at $\omega = \omega_a$ with width close $\omega_{g_2 g_1}$. The difference between the negative and positive-step, Eq. (17), shows a peak at $\omega = \omega_a$ and a Stokes peak at $\omega_a + \omega_{g_2 g_1}$. We assume that the molecule is initially in the g_1 state, meaning that the anti-Stokes processes are not possible.

The transmission signal for a narrow positive phase-pulse Eq. (9) $S(\omega; \phi_2(\omega, \tilde{\omega} + \frac{\Delta\omega}{2}, \tilde{\omega} - \frac{\Delta\omega}{2}))$ with $\tau = 0.5\text{cm}$ is shown in Fig. 11(d) for three values of $\tilde{\omega}$. The black-dashed line corresponds to the transmission spectrum Eq. (14) with $\phi = 0$. The spectrum for $\tilde{\omega} = 7825\text{cm}^{-1}$, shows two peaks at Ω_1 and $\tilde{\omega}$ with width close to $\omega_{g_2 g_1}$. The same two peaks appear for $\tilde{\omega} = 8150\text{cm}^{-1}$. When $\tilde{\omega} = \Omega_1$, there are two peaks at $\omega = \Omega_1, \Omega_1 + \omega_{g_2 g_1}$. For a negative phase-step, $\tau = -0.5\text{cm}^{-1}$, we see the same peaks, with slightly different line-shapes.

The difference between the positive and negative phase-pulse, Eq. (20) is shown in Fig. 11(f). For $\tilde{\omega} = 7825\text{cm}^{-1}$, there are four peaks, $\omega = \tilde{\omega}, \tilde{\omega} + \omega_{g_2 g_1}, \Omega_1, \Omega_1 + \omega_{g_2 g_1}$. The same peaks occur for $\tilde{\omega} = 8150\text{cm}^{-1}$. For $\tilde{\omega} = \Omega_1$ only two peaks occur $\omega = \Omega_1, \Omega_1 + \omega_{g_2 g_1}$. The Raman peaks at $\omega = \Omega_1 + \omega_{g_2 g_1}, \tilde{\omega} + \omega_{g_2 g_1}$ contain both absorption and emission features. Note that there are some wiggles on the signal in Figs. 11(d), (e). The numerical value of the integrations calculated in Eq. (9) is on the order 10^{-5} , which is relatively small. The accuracy of the numerical integration was

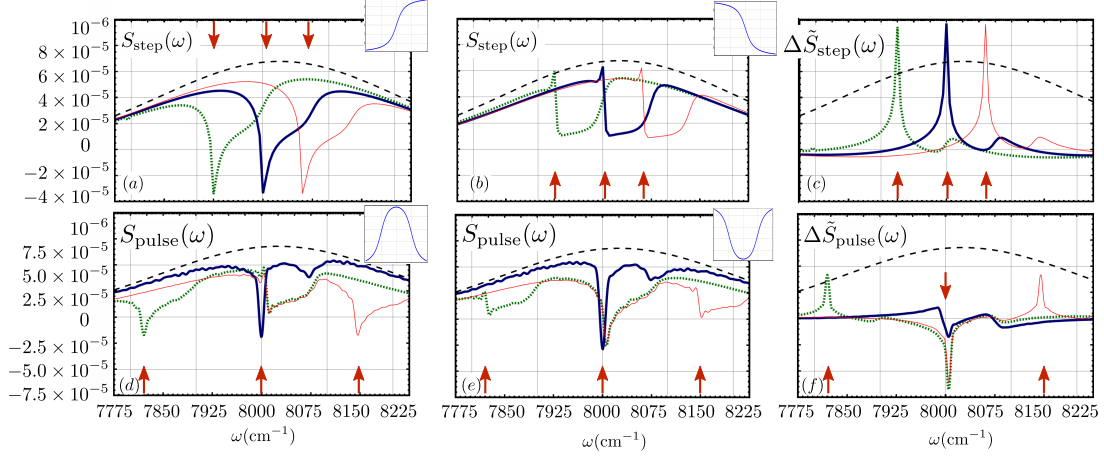


FIG. 11: (Color online) Top row: The transmission signal Eq. (9) with phase-step, $\phi_1(\omega, \omega_a)$, for three values of ω_a : (dashed-green) $\omega_a = 7925\text{cm}^{-1}$, (thick-blue) $\omega_a = \Omega_1$, (thin-red) $\omega_a = 8060\text{cm}^{-1}$. (a) $\tau_a = 0.5\text{cm}$. (b) $\tau_a = -0.5\text{cm}$. (c) Difference between (a) and (b), Eq. (17). Bottom row: The transmission signal with a phase-pulse $\phi_2(\omega, \tilde{\omega} + \frac{\Delta\omega}{2}, \tilde{\omega} - \frac{\Delta\omega}{2})$ with width $\Delta\omega = 10\text{cm}^{-1}$ and three values of pulse position $\tilde{\omega}$: (dashed-green) $\tilde{\omega} = 7825\text{cm}^{-1}$, (thick-blue) $\tilde{\omega} = \Omega_1$, (thin-red) $\tilde{\omega} = 8150\text{cm}^{-1}$, (d) $\tau = 0.5\text{cm}$. (e) $\tau = -0.5\text{cm}$. (f) Difference between (d) and (e), Eq. (20). The dashed-black line is the transmission spectrum with no phase $\phi = 0$. The red arrows marks the position of the phase-step. The insets show the shape of the phase-step or pulse.

set to 10^{-8} .

VI. DISCUSSION

We have simulated the nonlinear transmission signal of a broadband pulse with a phase-step and phase-pulse with finite-transition width. Two dimensional plots of the transmission signal vs. the transmitted frequency and the position of a π -step or pulse show diagonal peaks spread above and below the diagonal line. The transmission spectra show that the phase-step or narrow-

pulse can suppress certain quantum pathways. The diagonal peaks in the transmission spectra are sensitive to the phase sign. The TPA peaks are enhanced better for a negative step or narrow-pulse rather than for a positive. The peaks from the Stokes process are enhanced more for a positive step or narrow-pulse compared to a negative. We found that the sign of the pulse or step becomes relevant when the position of the step or pulse is close to the transition peak frequencies. A positive or negative phase-pulse selects particular peaks. The narrow phase-pulse suppressed the contributions from the diagrams (II) and (III) in Fig. 4, while the transmission spectra for the phase-step was dominated by the diagrams (II) and (III) in Fig. 4.

The difference between a positive and negative phase-step or phase-pulse shows peaks along the diagonal line. The arctan phase can be expanded as the sum of an even and odd functions. Subtracting the transmission signal with a positive and negative phase-step or pulses gives the spectra which is enhanced by the odd-spectral phase.

We compared two protocols for enhancing the TPA peaks in the transmission spectrum. Refs. [40] employed a wide pulse with the two phase-steps located at the two transition frequencies involved in the TPA. We plotted the two-dimensional transmission spectra for a variable pulse width in Fig. 8(b). However, the spectra showed that the TPA is enhanced either for a narrow-phase-pulse or with a negative going phase-step. The spectra did not show any peaks corresponding to a wide pulse with two phase-steps located at the two transition frequencies involved in the TPA. We compared this protocol to the phase-step and a narrow phase-pulse and showed that the step gave the best amplification of the pulse.

ACKNOWLEDGMENTS

We gratefully acknowledge the support of the Chemical Sciences, Geosciences and Biosciences Division, Office of Basic Energy Sciences, Office of Science, U.S. Department of Energy. We also wish to thank the National Science Foundation (Grant No. CHE-1058791).

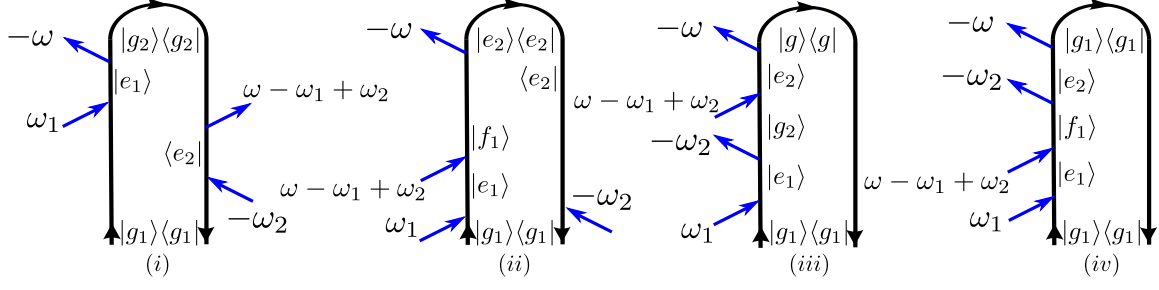


FIG. 12: (Color online) Loop diagrams for the frequency dispersed transmitted signal Eq. (5) expanded to third-order in H_{int} . The frequencies ω_1 and ω_2 correspond to the frequencies ω_1 and ω_2 in Eq. (A1).

Appendix A: Loop diagram expansion in $\chi^{(3)}$

The susceptibility Eq. (10) can be written in Hilbert space, corresponding the loop diagrams in Fig. 12, as

$$\begin{aligned} \chi^{(3)}(-\omega; \omega_1, -\omega_2, \omega - \omega_1 + \omega_2) = & \chi_i^{(3)}(-\omega; \omega_1, -\omega_2, \omega - \omega_1 + \omega_2) + \chi_{ii}^{(3)}(-\omega; \omega_1, -\omega_2, \omega - \omega_1 + \omega_2) \\ & + \chi_{iii}^{(3)}(-\omega; \omega_1, -\omega_2, \omega - \omega_1 + \omega_2) + \chi_{iv}^{(3)}(-\omega; \omega_1, -\omega_2, \omega - \omega_1 + \omega_2), \end{aligned} \quad (A1)$$

where

$$\chi_i^{(3)}(-\omega; \omega_1, -\omega_2, \omega - \omega_1 + \omega_2) = \left(\frac{-1}{2\pi\hbar}\right)^3 \sum_{g_i, e_i, f_i} V_{g_1 e_2} V_{e_2 g_2} V_{g_2 e_1} V_{e_1 g_1} G_{e_2}^\dagger(\omega_2) G_{g_2}^\dagger(-\omega + \omega_1) G_{e_1}(\omega_1), \quad (A2)$$

$$\chi_{ii}^{(3)}(-\omega; \omega_1, -\omega_2, \omega - \omega_1 + \omega_2) = \left(\frac{-1}{2\pi\hbar}\right)^3 \sum_{g_i, e_i, f_i} V_{g_1 e_2} V_{e_2 f_1} V_{f_1 e_1} V_{e_1 g_1} G_{e_2}^\dagger(\omega_2) G_{f_1}(\omega + \omega_2) G_{e_1}(\omega_1), \quad (A3)$$

$$\chi_{iii}^{(3)}(-\omega; \omega_1, -\omega_2, \omega - \omega_1 + \omega_2) = \left(\frac{-1}{2\pi\hbar}\right)^3 \sum_{g_i, e_i, f_i} V_{g_1 e_2} V_{e_2 g_2} V_{g_2 e_1} V_{e_1 g_1} G_{g_2}(\omega_1 - \omega_2) G_{e_2}(\omega) G_{e_1}(\omega_1), \quad (A4)$$

$$\chi_{iv}^{(3)}(-\omega; \omega_1, -\omega_2, \omega - \omega_1 + \omega_2) = \left(\frac{-1}{2\pi\hbar}\right)^3 \sum_{g_i, e_i, f_i} V_{g_1 e_2} V_{e_2 f_1} V_{f_1 e_1} V_{e_1 g_1} G_{e_2}(\omega) G_{f_1}(\omega + \omega_2) G_{e_1}(\omega_1). \quad (A5)$$

Equation (10) is similar to Eq. (A1), with the dephasing rates γ replaced with the inverse lifetimes.

Appendix B: Transmission spectra

The transmission spectrum $S_0(\omega)$ without pulse shaping is shown in Fig. 13(a). The three components $S_0^I(\omega)$, $S_0^{II}(\omega)$ and $S_0^{III}(\omega)$ of $S_0(\omega)$ are shown in Fig. 13(b)-(d), respectively. These components correspond to the signal from diagrams (I), (II), (III) in Fig. 4.

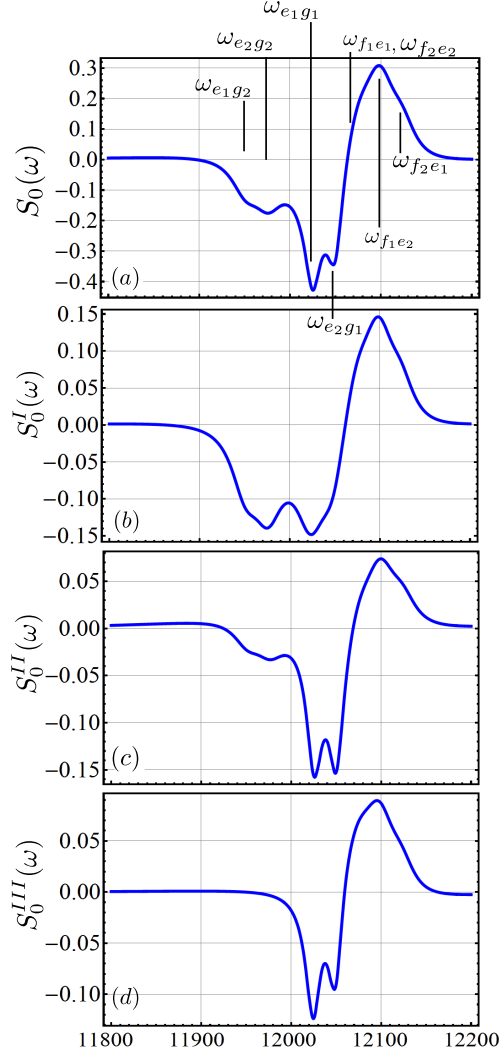


FIG. 13: (Color online) (a) The frequency dispersed transmission signal $S_0(\omega)$, Eq. (14) using a Gaussian pulse Eq. (8) for $\phi = 0$ $\sigma = 252\text{cm}^{-1}$ and $\Omega_1 = 12100\text{cm}^{-1}$. The components of $S_0(\omega)$ (b) $S_0^I(\omega)$, (c) $S_0^{II}(\omega)$, (d) $S_0^{III}(\omega)$ corresponding to the susceptibility components, Eq. (10).

The two-dimensional frequency dispersed transmission signal

$$\Delta S_{\text{step}}^i(\omega; \omega_a) = S^i(\omega; \phi_1(\omega, \omega_a, \tau_a)) - S_0^i(\omega), \quad (\text{B1})$$

is plotted in the first two columns of Fig. 14. The index $i = I, II, III$ represents the signal from diagrams (I), (II), (III) in Fig. 4, respectively. The first column corresponds to a positive phase-step $\tau_a = 0.5\text{cm}$ and the second column to a negative phase-step $\tau_a = -0.5\text{cm}$. The difference transmission signal with a negative and positive phase-step

$$\Delta\tilde{S}_{\text{step}}^i(\omega; \omega_a) = S(\omega; \phi_1(\omega, \omega_a, -\tau_a)) - S(\omega; \phi_1(\omega, \omega_a, \tau_a)) \quad (\text{B2})$$

is plotted in the third column of Fig. 14. The vertical black-dashed lines mark the positions of the transition peaks. The first three rows corresponds the transmission signal components from the ladder diagrams in Fig. 4(I), (II), (III), respectively. The fourth row corresponds to the total transmission signal. The sum

$$\Delta S_{\text{step}}(\omega; \omega_a) = \Delta S_{\text{step}}^I(\omega; \omega_a) + \Delta S_{\text{step}}^{II}(\omega; \omega_a) + \Delta S_{\text{step}}^{III}(\omega; \omega_a) \quad (\text{B3})$$

is plotted Figs. 14(j) (k), for a positive and negative step, respectively. The difference between (j) and (k), or the sum

$$\Delta\tilde{S}_{\text{step}}(\omega; \omega_a) = \Delta\tilde{S}_{\text{step}}^I(\omega; \omega_a) + \Delta\tilde{S}_{\text{step}}^{II}(\omega; \omega_a) + \Delta\tilde{S}_{\text{step}}^{III}(\omega; \omega_a) \quad (\text{B4})$$

is plotted in Fig. 14(l).

The difference transmission spectrum for a narrow phase-pulse with width $\Delta\omega = 10\text{cm}^{-1}$ is plotted in Fig. 15. The difference

$$\Delta S_{\text{pulse}}^i(\omega; \tilde{\omega}) = S^i(\omega; \phi_2(\omega, \tilde{\omega} + \frac{\Delta\omega}{2}, \tilde{\omega} - \frac{\Delta\omega}{2}, \tau)) - S_0^i(\omega), \quad (\text{B5})$$

is displayed in the first two columns of Fig. 15, where the index i can be I, II , or III . The first and second column corresponds to a positive and negative pulse, respectively. The difference in the transmission signal with a negative and positive pulse

$$\Delta\tilde{S}_{\text{pulse}}^i(\omega; \tilde{\omega}) = S^i(\omega; \phi_2(\omega, \tilde{\omega} + \frac{\Delta\omega}{2}, \tilde{\omega} - \frac{\Delta\omega}{2}, -\tau)) - S^i(\omega; \phi_2(\omega, \tilde{\omega} + \frac{\Delta\omega}{2}, \tilde{\omega} - \frac{\Delta\omega}{2}, \tau)) \quad (\text{B6})$$

is plotted in the third column of Fig. 15. The sum

$$\Delta S_{\text{pulse}}(\omega; \omega_a) = \Delta S_{\text{pulse}}^I(\omega; \omega_a) + \Delta S_{\text{pulse}}^{II}(\omega; \omega_a) + \Delta S_{\text{pulse}}^{III}(\omega; \omega_a) \quad (\text{B7})$$

is plotted Figs. 15(j) (k), for a positive and negative step, respectively. The difference between (j) and (k), or the sum

$$\Delta\tilde{S}_{\text{pulse}}(\omega; \omega_a) = \Delta\tilde{S}_{\text{pulse}}^I(\omega; \omega_a) + \Delta\tilde{S}_{\text{pulse}}^{II}(\omega; \omega_a) + \Delta\tilde{S}_{\text{pulse}}^{III}(\omega; \omega_a) \quad (\text{B8})$$

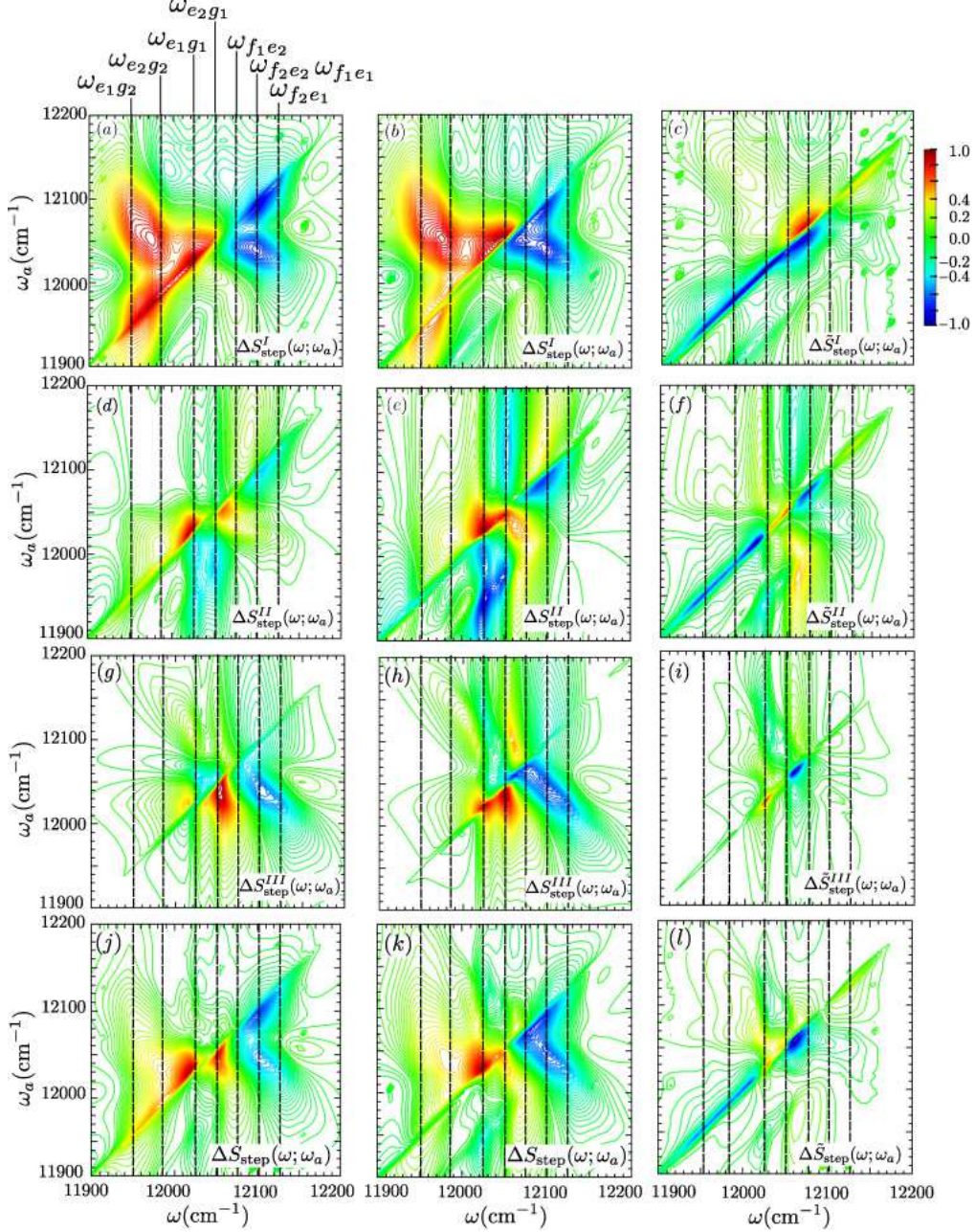


FIG. 14: (Color online) The two-dimensional frequency dispersed difference-transmission signal with phase $\phi_1(\omega, \omega_a)$, vs phase-step position, ω_a . (Left column) Positive step, $\Delta S_{\text{step}}^i(\omega, \omega_a)$, Eq. (B1) with $\tau_a = 0.5\text{cm}$; (Middle column) negative step, $\Delta S_{\text{step}}^i(\omega, \omega_a)$, Eq. (B1) with $\tau_a = -0.5\text{cm}$; (Right column) difference between a positive and negative step, $\Delta \tilde{S}_{\text{step}}^i(\omega, \omega_a)$ Eq. (B2). (First row) S_{step}^I ; (Second row) S_{step}^{II} ; (Third row) S_{step}^{III} ; (Fourth row) the total transmission signal, (j), (k) Eq. (B3); (l) Eq. (B4) The vertical dashed-black lines mark the transition frequencies.

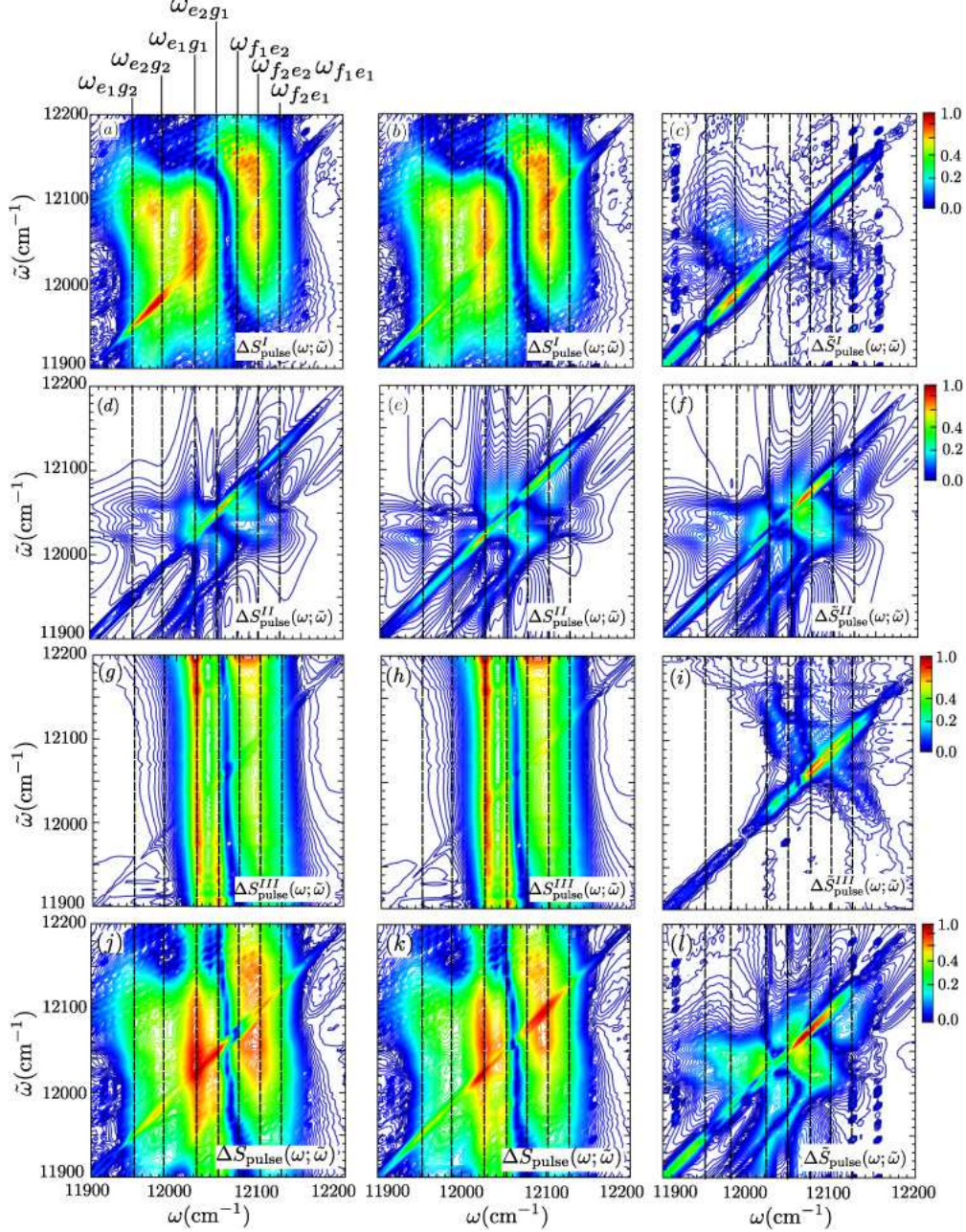


FIG. 15: (Color online) The two-dimensional frequency dispersed difference-transmission signal vs the phase-pulse, $\phi_2(\omega, \tilde{\omega} + \frac{\Delta\omega}{2}, \tilde{\omega} - \frac{\Delta\omega}{2})$, position $\tilde{\omega}$, with width $\Delta\omega = 10\text{cm}^{-1}$. (Left column)

Positive pulse, $\Delta S_{\text{pulse}}^i(\omega, \tilde{\omega})$; Eq. (B5) with $\tau = 0.5\text{cm}$, (Middle column) negative pulse, $\Delta S_{\text{pulse}}^i(\omega, \tilde{\omega})$; Eq. (B5) with $\tau = -0.5\text{cm}$; (Right column) difference between a positive and negative pulse, $\Delta \tilde{S}_{\text{pulse}}^i(\omega, \tilde{\omega})$ Eq. (B6). (First row) S_{pulse}^I ; (Second row) S_{pulse}^{II} ; (Third row) S_{pulse}^{III} ; (Fourth row) the total transmission signal, (j), (k) Eq. (B7); (l) Eq. (B8). The vertical dashed-black lines mark the transition frequencies.

is plotted in Fig. 15(1).

-
- [1] S. A. Rice, “New ideas for guiding the evolution of a quantum system,” *Science*, vol. 258, pp. 412–413, Oct. 1992. PMID: 17833135.
 - [2] W. S. Warren, H. Rabitz, and M. Dahleh, “Coherent control of quantum dynamics: The dream is alive,” *Science*, vol. 259, pp. 1581–1589, Mar. 1993. PMID: 17733021.
 - [3] E. M. Grumstrup, S.-H. Shim, M. A. Montgomery, N. H. Damrauer, and M. T. Zanni, “Facile collection of two-dimensional electronic spectra using femtosecond pulse-shaping technology,” *Opt. Express*, vol. 15, pp. 16681–16689, Dec. 2007.
 - [4] S.-H. Shim and M. T. Zanni, “How to turn your pumpprobe instrument into a multidimensional spectrometer: 2D IR and vis spectroscopies via pulse shaping,” *Phys. Chem. Chem. Phys.*, vol. 11, pp. 748–761, Feb. 2009.
 - [5] D. J. Tannor and S. A. Rice, “Coherent pulse sequence control of product formation in chemical reactions,” in *Advances in Chemical Physics* (I. Prigogine and S. A. Rice, eds.), p. 441523, John Wiley & Sons, Inc., 2007.
 - [6] D. Lorenc, D. Velic, A. N. Markevitch, and R. J. Levis, “Adaptive femtosecond pulse shaping to control supercontinuum generation in a microstructure fiber,” *Optics Communications*, vol. 276, pp. 288–292, Aug. 2007.
 - [7] S. A. Rice and M. Zhao, *Optical control of molecular dynamics*. New York: John Wiley, 2000.
 - [8] B. Bederson and H. Walther, *Advances in Atomic, Molecular, and Optical Physics*. Gulf Professional Publishing, 2001.
 - [9] A. Assion, T. Baumert, M. Bergt, T. Brixner, B. Kiefer, V. Seyfried, M. Strehle, and G. Gerber, “Control of chemical reactions by feedback-optimized phase-shaped femtosecond laser pulses,” *Science*, vol. 282, pp. 919–922, Oct. 1998. PMID: 9794756.
 - [10] C. Daniel, J. Full, L. Gonzalez, C. Lupulescu, J. Manz, A. Merli, t. Vajda, and L. Wste, “Deciphering the reaction dynamics underlying optimal control laser fields,” *Science*, vol. 299, pp. 536–539, Jan. 2003. PMID: 12543966.
 - [11] A. M. Weiner, “Ultrafast optical pulse shaping: A tutorial review,” *Optics Communications*, vol. 284, pp. 3669–3692, July 2011.
 - [12] D. Goswami, “Optical pulse shaping approaches to coherent control,” *Physics Reports*, vol. 374,

pp. 385–481, Feb. 2003.

- [13] J.-X. Cheng and X. S. Xie, *Coherent Raman Scattering Microscopy*. CRC Press, October 29 2012.
- [14] V. V. Lozovoy and M. Dantus, “Systematic control of nonlinear optical processes using optimally shaped femtosecond pulses,” *Chemphyschem*, vol. 6, pp. 1970–2000, Oct. 2005. PMID: 16208734.
- [15] J. N. Eckstein, A. I. Ferguson, and T. W. Hensch, “High-resolution two-photon spectroscopy with picosecond light pulses,” *Phys. Rev. Lett.*, vol. 40, pp. 847–850, Mar. 1978.
- [16] *Femtosecond Optical Frequency Comb: Principle, Operation and Applications*.
- [17] D. Meshulach and Y. Silberberg, “Coherent quantum control of multiphoton transitions by shaped ultrashort optical pulses,” *Phys. Rev. A*, vol. 60, pp. 1287–1292, Aug. 1999.
- [18] Y. Silberberg, “Quantum coherent control for nonlinear spectroscopy and microscopy,” *Annual Review of Physical Chemistry*, vol. 60, no. 1, pp. 277–292, 2009. PMID: 18999997.
- [19] I. Pastirk, J. Dela Cruz, K. Walowicz, V. Lozovoy, and M. Dantus, “Selective two-photon microscopy with shaped femtosecond pulses,” *Opt. Express*, vol. 11, pp. 1695–1701, July 2003.
- [20] S. Zhang, C. Lu, T. Jia, J. Qiu, and Z. Sun, “Control of resonance enhanced multi-photon ionization photoelectron spectroscopy by phase-shaped femtosecond laser pulse,” *The Journal of Chemical Physics*, vol. 137, p. 174301, Nov. 2012.
- [21] D. Oron, N. Dudovich, D. Yelin, and Y. Silberberg, “Quantum control of coherent anti-stokes raman processes,” *Physical Review A*, vol. 65, Apr. 2002.
- [22] T. Polack, D. Oron, and Y. Silberberg, “Control and measurement of a non-resonant raman wavepacket using a single ultrashort pulse,” *Chemical Physics*, vol. 318, pp. 163–169, Nov. 2005.
- [23] S.-H. Lim, A. G. Caster, and S. R. Leone, “Single-pulse phase-control interferometric coherent anti-stokes raman scattering spectroscopy,” *Phys. Rev. A*, vol. 72, p. 041803, Oct. 2005.
- [24] D. Oron, N. Dudovich, and Y. Silberberg, “All-optical processing in coherent nonlinear spectroscopy,” *Phys. Rev. A*, vol. 70, p. 023415, Aug. 2004.
- [25] S. Roy, P. Wrzesinski, D. Pestov, T. Gunaratne, M. Dantus, and J. R. Gord, “Single-beam coherent anti-stokes raman scattering spectroscopy of n_2 using a shaped 7 fs laser pulse,” *Applied Physics Letters*, vol. 95, p. 074102, Aug. 2009.
- [26] D. Oron, N. Dudovich, D. Yelin, and Y. Silberberg, “Narrow-band coherent anti-stokes raman signals from broad-band pulses,” *Phys. Rev. Lett.*, vol. 88, p. 063004, Feb. 2002. PMID: 11863805.
- [27] S. Postma, A. C. W. van Rhijn, J. P. Korterik, P. Gross, J. L. Herek, and H. L. Offerhaus, “Application of spectral phase shaping to high resolution CARS spectroscopy,” *Optics Express*, vol. 16, p. 7985,

May 2008.

- [28] N. Dudovich, D. Oron, and Y. Silberberg, “Single-pulse coherently controlled nonlinear raman spectroscopy and microscopy,” *Nature*, vol. 418, pp. 512–514, Aug. 2002.
- [29] D. Oron, N. Dudovich, and Y. Silberberg, “Single-pulse phase-contrast nonlinear raman spectroscopy,” *Phys. Rev. Lett.*, vol. 89, p. 273001, Dec. 2002.
- [30] P. Nuernberger, G. Vogt, T. Brixner, and G. Gerber, “Femtosecond quantum control of molecular dynamics in the condensed phase,” *Physical Chemistry Chemical Physics*, vol. 9, no. 20, p. 2470, 2007.
- [31] B. D. Bruner, H. Suchowski, N. V. Vitanov, and Y. Silberberg, “Strong-field spatiotemporal ultrafast coherent control in three-level atoms,” *Physical Review A*, vol. 81, p. 063410, June 2010.
- [32] R. J. Levis, G. M. Menkir, and H. Rabitz, “Selective bond dissociation and rearrangement with optimally tailored, strong-field laser pulses,” *Science*, vol. 292, pp. 709–713, Apr. 2001. PMID: 11283357.
- [33] T. Baumert, T. Brixner, V. Seyfried, M. Strehle, and G. Gerber, “Femtosecond pulse shaping by an evolutionary algorithm with feedback,” *Appl Phys B*, vol. 65, pp. 779–782, Dec. 1997.
- [34] M. A. Montgomery, R. R. Meglen, and N. H. Damrauer, “General method for reducing adaptive laser pulse-shaping experiments to a single control variable,” *J. Phys. Chem. A*, vol. 111, pp. 5126–5129, June 2007.
- [35] T. Hornung, R. Meier, D. Zeidler, K.-L. Kompa, D. Proch, and M. Motzkus, “Optimal control of one- and two-photon transitions with shaped femtosecond pulses and feedback,” *Appl Phys B*, vol. 71, pp. 277–284, Sept. 2000.
- [36] R. S. Judson and H. Rabitz, “Teaching lasers to control molecules,” *Phys. Rev. Lett.*, vol. 68, pp. 1500–1503, Mar. 1992.
- [37] T. Bayer, M. Wollenhaupt, C. Sarpe-Tudoran, and T. Baumert, “Robust photon locking,” *Phys. Rev. Lett.*, vol. 102, p. 023004, Jan. 2009.
- [38] S. Mukamel, “Superoperator representation of nonlinear response: Unifying quantum field and mode coupling theories,” *Phys. Rev. E*, vol. 68, p. 021111, Aug 2003.
- [39] U. Harbola and S. Mukamel, “Superoperator nonequilibrium green’s function theory of many-body systems; applications to charge transfer and transport in open junctions,” *Phys. Rep.*, vol. 465, pp. 191–222, 2008.
- [40] N. Dudovich, B. Dayan, S. M. Gallagher Faeder, and Y. Silberberg, “Transform-limited pulses are not optimal for resonant multiphoton transitions,” *Phys. Rev. Lett.*, vol. 86, pp. 47–50, Jan. 2001.